

EUROPEAN ORGANIZATION FOR NUCLEAR RESEARCH

Proposal to the ISOLDE and Neutron Time-of-Flight Committee

$^{33}\text{S}(n,\alpha)^{30}\text{Si}$ cross section measurement at n_TOF EAR2.

[submission date: 03/06/2015]

Javier Praena^{1,2}, Ignacio Porras², Marta Sabaté-Gilarte^{3,4}, José Manuel Quesada³,
for the n_TOF collaboration

- 1) Universidad de Granada, Spain
- 2) Centro Nacional de Aceleradores (US-JA-CSIC), Sevilla, Spain
- 3) Universidad de Sevilla, Spain
- 4) CERN, Switzerland

Spokesperson(s): Javier Praena (jpraena@us.es)
Ignacio Porras (porras@ugr.es)

Technical coordinator: Oliver Aberle

Abstract

This proposal is a continuation and a consequence of the successful experiment performed in 2012 at n_TOF EAR1 (CERN-INTC-2012-006/INTC-P-322) in the light of the results obtained in the data analysis. The main goal of our experiment at EAR-1 was to clarify the discrepancy in the resonance region between the scarce experiment data. For this reason we took advantage of the high-energy resolution available at EAR-1 and we measured the $^{33}\text{S}(n,\alpha)^{30}\text{Si}$ cross-section with $^{10}\text{B}(n,\alpha)^7\text{Li}$ as reference. We have found a good agreement with Wagemans *et al.*. Moreover, we have also obtained data below 10 keV (down to 1 eV), in a region where no previous data were known (except the thermal point), but these are not conclusive. Some effects might influence our data below 10 keV, in particular a high general electronic noise level in addition to an electronic noise signal induced by the PS accelerator signal. Furthermore, the background study was not optimized by a measurement without target for all detectors. In this situation, the extrapolation of EAR-1 data from 10 keV to thermal neutron energy is highly uncertain, and would lead to values at the thermal point more than two orders of magnitude higher with respect to the reported values. We propose to complete the measurement of the $^{33}\text{S}(n,\alpha)^{30}\text{Si}$ cross-section in EAR-2. The work performed during the EAR-2 commissioning on the detectors should improve the quality of the data below 10 keV hopefully providing a reliable shape and value of the $^{33}\text{S}(n,\alpha)^{30}\text{Si}$ cross-section below 10 keV. We will take advantage of the improved signal-to-noise ratio, a better background characterization and, especially, the much higher flux of low energy neutrons in EAR-2, as compared with EAR-1. In addition the same digitizers of the data acquisition system allow reaching the thermal neutron energy directly without the need for extrapolation. This data might be relevant for applications to medical physics, also the proposed setup will allow studying nuclear structure effects related to the anisotropy in the forward and backward alpha emission suggested by Wiechers *et al.*

Requested protons: $2 \cdot 10^{18}$ protons on target.

Experimental area: EAR-2

1. SCIENTIFIC MOTIVATIONS

The present proposal is a continuation of the first experiment at n_TOF aiming at measuring (n,α) cross sections [1]. We will only briefly review the motivations here. The $^{33}\text{S}(n,\alpha)$ cross-section is involved in the origin of ^{36}S , which is an open question, it is of interest in boron neutron capture therapy of head and neck cancer, and may provide information on nuclear structure and fundamental nuclear physics.

In nuclear astrophysics, ^{33}S is of interest for the nucleosynthesis of ^{36}S . The neutron-rich isotopes ^{36}S , ^{40}Ar and ^{48}Ca are bypassed by charge particle induced reactions and ^{33}S belongs to the nuclear reaction net that could produce ^{36}S , in particular the $^{33}\text{S}(n,\alpha)$ cross-section. Auchampaugh *et al* [2] obtained in a time-of-flight (TOF) measurement the Maxwellian Average Cross Section (MACS) of $^{33}\text{S}(n,\alpha)$ as a function of the energy, with a value of (690 ± 170) mb at $kT=30$ keV. That value corresponded to an overproduction of the ^{36}S in the universe. Wagemans *et al* [3] obtained by TOF a value of (227 ± 20) mb reducing this overproduction but with discrepant resonance parameters relate to those of Coddens *et al*. [4]. Later Schatz *et al* [5] obtained (175 ± 9) mb for the MACS at $kT=25$ keV by the activation technique, that extrapolated to the standard *s*-process temperature $kT=30$ keV gave a value of 181 mb, which is in better agreement with the results of [3]. The measurement of the MACS of $^{34}\text{S}(n,\gamma)$ at $kT=25$ keV by Reifarh *et al* [6] provided a value which made the ^{34}S a possible bottleneck in the path and a consequently accumulation of ^{34}S , reducing the *s*-process contribution of the total ^{36}S . Thus, the origin of ^{36}S remains an open question.

The possible use of ^{33}S in Boron Neutron Capture Therapy (BNCT) was proposed in [7]. Although the research in this field is multidisciplinary, the study of the $^{33}\text{S}(n,\alpha)$ cross section is mandatory for determining the delivered dose to tumours [8,9]. BNCT is an experimental radiotherapy that makes use of low energy neutrons and has produced recently very promising clinical results in cancer of very bad prognosis [10]. BNCT consists of the injection of a ^{10}B carrier, with high tumour-cell specificity and subsequent the irradiation of the tumour area with neutrons of epithermal energy. In BNCT, the neutrons are moderated by the tissue and reach the boron doped-tumour with thermal energy. Then the alpha particles (1.47 MeV) and ^7Li nucleus (0.8 MeV) ejected in the reaction of the neutrons with boron and produce a strong damage in the cell sparing nearby ones because of their short range (of the order of the cell size). BNCT is therefore considered as a cell targeted internal heavy-ion therapy. Up to now BNCT clinical trials have been performed with neutron beams from nuclear research reactors but at present a few accelerator-based neutron sources are being constructed for BNCT purposes [10]. Conventional BNCT has been used as treatment mainly in glioblastoma (Figure 1 on the left) and recurrent head and neck cancers (Figure 1 on the right) [10]. It must be stressed that BNCT represents the unique possibility for locally recurrent cancers because of the low dose delivered to healthy tissue [10]. Moreover, BNCT treatment is performed in only one or two sessions.

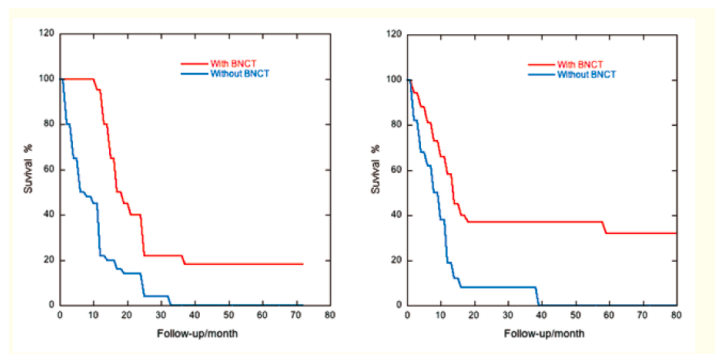


Figure 1. Kaplan-Meier survival plots (% survival as a function of time) for patients treated with BNCT compared to other treatments [10]. Glioblastoma on the left and head and neck on the right, red lines means survival with BNCT and blue line without BNCT.

One of the possible applications of ^{33}S is in the treatment of recurrent head and neck cancers that frequently grow to the skin. In these cases the dose delivered to the tumour is very low in the 2-3 first centimetres because a moderation of the neutrons is necessary before they could react with ^{10}B . Therefore if a ^{33}S carrier is delivered

to the tumour in addition to ^{10}B carrier the dose will be significantly increased from the skin surface. It must be stressed that natural sulphur is already present in compounds used in chemotherapy and ^{35}S has been used in medical physics [11][12]. Figure 2 shows the simulated dose in tumour vs. healthy tissue (red symbols) delivered by a neutron beam of 13.5 keV of $10^{10} \text{ ns}^{-1}\text{cm}^2$ when S-33 and/or B-10 are present in the tumour. The calculation is based on a detailed MCNPX neutron transport simulations with dose estimations based on kerma factors. The tumour was mimicked by means of a cylinder of ICRU-4 tissue [13] doped with B-10 concentrations as [8] and S-33 with concentrations based on [11][12]. We use the most conservative values of the cross-section. From 13.5 keV to 10 keV we use Wagemans *et al* [3] cross-section and from 10 keV to thermal we used the ENDF/B-VII.1 evaluation. The results of the simulations allow studying ^{33}S as a possible cooperative target in BNCT treatments of recurrent head and neck cancers. More details can be found in [8][9]. Although the figure corresponds to an ideal neutron source, additional ongoing simulations show also important dose enhancement in the tumour for more realistic spectra of the neutron source.

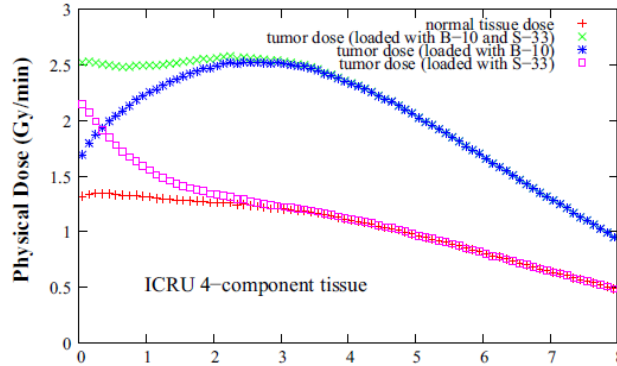


Figure 2. Dose vs. depth (cm) delivered by a neutron beam of 13.5 keV, $10^{10} \text{ ns}^{-1}\text{cm}^2$, when S-33 and/or B-10 are delivered to the ICRU-4 tissue in the selective concentrations based on [10,11,12].

We will show in the following section the cross-section extracted from the experiment at EAR-1 with our data analysis. It must be stressed that simulations of the dose considering our $^{33}\text{S}(n,\alpha)$ cross section data might improve the dose by a factor 10 to that of Figure 2. Our data at low energy, as discussed below, are not conclusive because they may be affected by unexpected electronic noise (pickup of the PS signal), and by other sources of background. Furthermore, data were collected only down to 1 eV. In light of the above considerations, it is very important to determine the value and shape of the cross-section below 10 keV. For this measurement is not mandatory a high-energy resolution while it is more important to count on a high flux at low neutron energies. At EAR-2 neutron flux below 1 eV is enhanced 10 times more than at EAR-1.

2. RESULTS OF THE $^{33}\text{S}(n,\alpha)^{30}\text{Si}$ EXPERIMENT AT n_TOF EAR-1

The experimental setup used in 2012 consisted of an ionization chamber with Micromegas detectors. The Micromegas detector concept is similar to the fast ionization chamber [14]. The sample coating was a challenge since ^{33}S is an extremely volatile and reactive material. Previous experiments had suffered of the sublimation of ^{33}S in vacuum [3]. A successful technique was developed by VSC group at CERN based on the thermal evaporation of ^{33}S powder onto a substrate of Cu-Ti-Cr-Kapton. The characterization by Rutherford backscattering technique was performed at CNA (Sevilla, Spain) [1]. We used 3.7 MeV alpha beam as a compromise between perfect discrimination of the ^{33}S from the rest of the elements present in the sample, and pure Rutherford cross-section. The sample thickness Δx (at/barn) was determined as given in Table 1. We found that each sample was homogeneous within 3% of the mass. In order to be conservative we assign 4% of uncertainty in the mass of the samples. Table 1 shows the result of the RBS characterization of the samples.

	Sample 1	Sample 2	Sample 3	Sample 4	Sample 5	Sample 6	Sample 7	Sample 8
Mass ($\cdot 10^{-7}$ at/b)	3.79 \pm 0.15	3.49 \pm 0.14	2.59 \pm 0.10	2.15 \pm 0.09	2.77 \pm 0.11	3.65 \pm 0.15	3.76 \pm 0.15	3.58 \pm 0.14

Table 1. Mass of the samples determined by Rutherford backscattering technique.

Figure 3 shows our result of the $^{33}\text{S}(n,\alpha)$ cross section with 1000 bins per decade using the standard $^{10}\text{B}(n,\alpha)$ cross-section as reference. Figure 4 shows a comparison between our data (black points), Wagemans *et al.* [3] (blue points), ENDF/B-VII.1 evaluation (green line), the resulting $1/v$ extrapolation of the data (red line) and the existing experimental values at thermal energy [15][16][17][18].

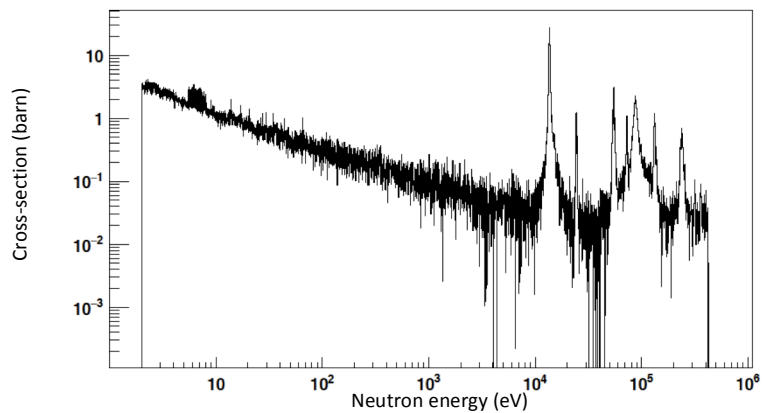


Figure 3. Experimentally obtained cross section (barn) vs. neutron energy (eV) at n_TOF EAR-1.

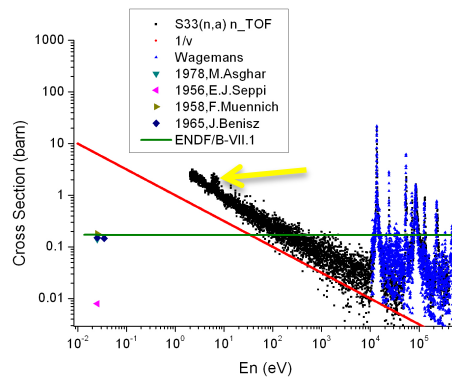


Figure 4. Experimental cross section (b) vs. neutron energy (eV) at n_TOF EAR-1 (black points) compared with Wagemans *et al.* [3] (blue points); $1/v$ extrapolation of the data (red line) and the ENDF/B-VII.1 evaluation (green line) of the $^{33}\text{S}(n,\alpha)$ cross-section are included. Yellow arrow indicates a possible “echo” due to the PS signal.

In spite of the fluctuations of the cross-section below 10 keV the slope clearly deviates from the expected $1/v$ shape. The resulting extrapolation of the data to thermal energy provides a value two order of magnitude higher than the experiment values. This result is very questionable and it must redetermined with a new measurement with an improved signal-to-noise ratio, wider energy range (down to thermal energy), reduced background, higher statistics at low energy and the absence of a spurious PS accelerator signal induced in the electronics.

At n_TOF-EAR1 during 2012 campaign a spurious signal related to the PS operation was present for every proton pulse. This signal occurred at a time-of-flight equivalent to a low energy neutron with a maximum value of 1eV but some “echoes” (orders of magnitude lower) of the signal can also be found at different equivalent neutron energies. For instance, a probably echo is the signal at 10 eV that can be noticed in Figure 4. This strong limitation on the neutron energy range makes more difficult the determination of the cross-section shape at low energies more difficult. Figure 5 shows a 2D plot of Amplitude versus TOF for the $^{10}\text{B}(n,\alpha)$ reaction used as reference in the experiment in 2012 (on the left) and for the $^{33}\text{S}(n,\alpha)$ (on the right). The PS signal is evident (black arrows).

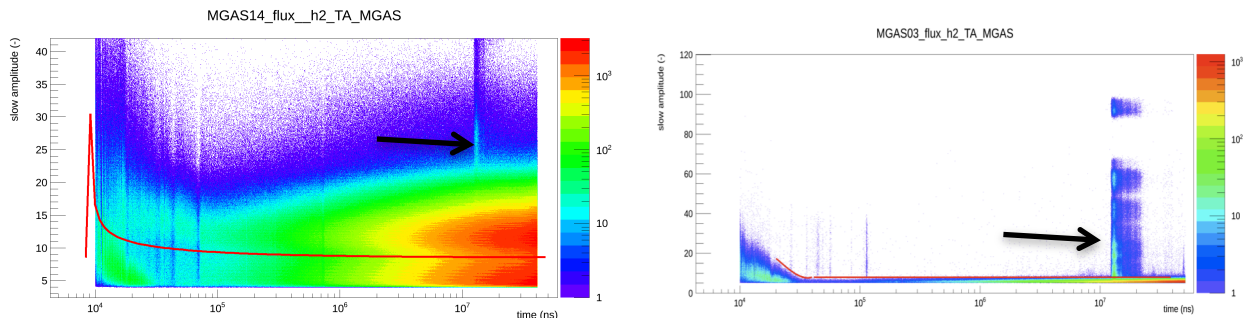


Figure 5. 2D plot of Amplitude versus TOF for the $^{10}\text{B}(n,\alpha)$ reaction used as reference (left) and for the $^{33}\text{S}(n,\alpha)$ (right) in the experiment in 2012. The black arrows indicate the PS signal in large TOF that corresponds approximately to 1 eV neutron energy.

During the commissioning at EAR-2 in 2015 a large effort was devoted to optimizing the shielding and grounding of the detectors and front-end electronics. This resulted in a very low level of the electronic noise. Furthermore, the spurious signal from the PS was not observed. Figure 6 shows 2D amplitude versus neutron energy obtained at EAR-2 with a Micromegas detector and a Kapton sample. It must be noticed the absence of the PS signal that correspond to 1 eV neutrons as it has been mentioned before. Above 10^5 eV the large signals correspond to the effect of the gamma-flash in the Micromegas detector.

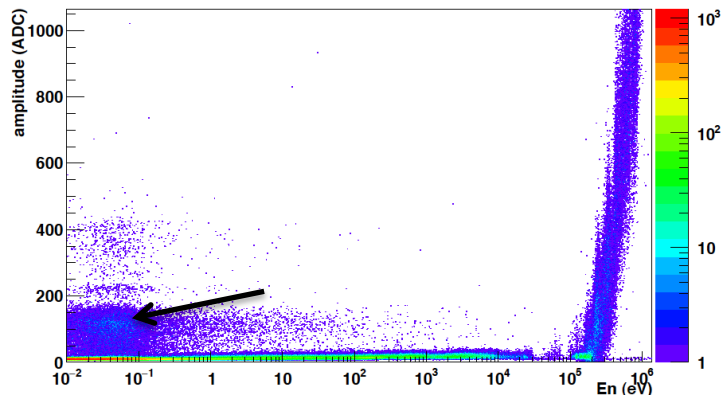


Figure 6. 2D Area of the signal versus neutron energy obtained at EAR-2 with a Micromegas detector and a Kapton sample obtained during the commissioning and the work of improvement in the signal-to-noise ratio. The absence of the PS signal must be stressed. Black arrow indicates the region corresponding to 400-600 keV of energy loss in the drift of the Micromegas.

The work performed during the commissioning of the new experimental area in the use of a new preamplifier for Micromegas detector result in a much-improved signal-to-background ratio. Figure 6 shows the results of a preliminary test on the possibility to perform at n_TOF measurement of (n,p) reactions, see our Letter of Intent [19]. The calibration performed during this test shows that particles of 400-600 keV (black arrow) can be

measured with the new Micromegas setup, well below the energy of the alpha particles from the $^{33}\text{S}(n,\alpha)$ reaction.

The third issue we have mentioned is the physical background. In the experiment at EAR-1 in 2012 we included two blank samples in order to study the background. A blank is a sample identical to that of ^{33}S before the evaporation of ^{33}S . Unfortunately the different behavior of each Micromegas detector does not allow a reliable subtraction of the background. We propose to estimate the physical background with blank samples and the same detector used for measuring the $^{33}\text{S}(n,\alpha)$ cross-section.

The improvements of the setup together with a higher statistics at EAR-2 below 10 keV, may allow studying interesting effect related to nuclear structure. Few states of the S-34 nucleus have been measured and a noticeable anisotropy in the angular distribution of the reaction between the forward and backward emission has been reported by Wiechers *et al.* [20] in inverse kinematics experiments such $^{30}\text{Si}(\alpha,n)^{33}\text{S}$ and $^{30}\text{Si}(\alpha,\gamma)^{34}\text{S}$. In particular “non-symmetric shapes and general forward peaking. These futures are suggestive of a direct reaction mechanism rather than that of compound nucleus formation”. To better study this effect, we propose to rotate the chamber after half of the protons to compensate for possible systematic effects related to the detector efficiency or to the sample thickness so that forward sample/detector will become backward and vice versa. In case this anisotropy would be confirmed it could be studied by means of a semi realistic model including nucleon-nucleon interaction and the mean field effects of the nuclear interaction described with a deformed mean field and alpha cluster formation [21].

3. COUNTING RATE ESTIMATION AT EAR-2 AND PROPOSED SETUP

We have shown in this document that the data collected on $^{33}\text{S}(n,\alpha)^{30}\text{Si}$ cross-section in EAR-1 below 10 keV are not conclusive because they are affected by a residual electronic noise, and a non-optimized signal-to-background ratio. For this reason the count rate estimation for the new proposal has been performed with 3 existing evaluations that provide the largest and lowest values of the $^{33}\text{S}(n,\alpha)$ cross-section, see Figure 7. In Figure 4, we already compared the ENDF/B-VII.1 evaluation and our data. The count rate has been estimated with the neutron flux at EAR-2 and a sample thickness of $3e-7$ at/b. The International Commission on Radiation Units and Measurements (ICRU) recommends that the radiation dose delivered should be within 5% of the prescribed dose [13]. This means that uncertainty at each step within the treatment process, including cross-section data should be significantly smaller than 5%. **We request 2e18 protons** in order to have less than 5% statistical uncertainty in the most significant neutron energy region with a low-energy resolution of 10 bin per decade which is enough to fulfil the goals of the present proposal. We propose a new configuration of the experiment at EAR-2 relative to EAR-1, the whole chamber will be rotated in the middle of the experiment therefore forward sample/detector will become backward and vice versa, in order to study nuclear structure effects.

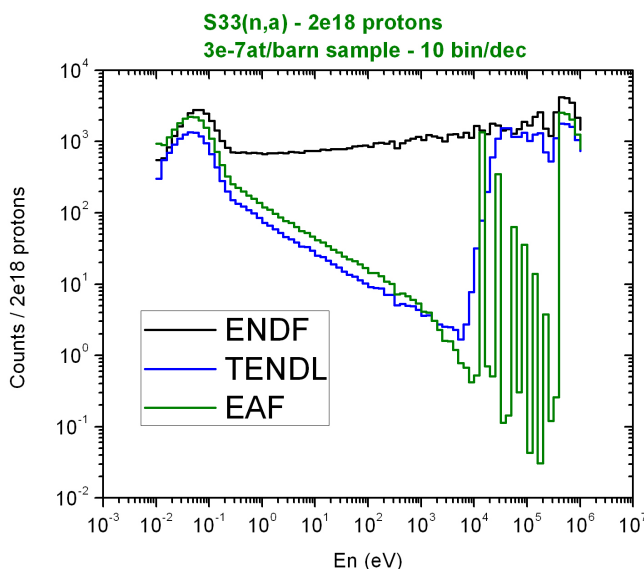


Figure 7: Expected counting based on ENDF/B-VII.1, EAF-2010 and TENDL-2012 considering 2e18 protons and a ^{33}S sample as the one used in the experiment in 2012. Resonances are not resolved in the ENDF/B-VII.1 because are not present in the evaluation but it should be resolved at EAR-2 with enough resolution as it can be seen from the EAF-2010 evaluation.

4. CONCLUSIONS

In the light of the results of the experiment performed at EAR-1 in 2012, we propose to complete the measurement of the $^{33}\text{S}(n,\alpha)^{30}\text{Si}$ cross-section in EAR-2. The new data would complement and complete the results obtained in the first measurement, providing indications on the cross section from thermal energy to 10 keV, a region where no data are presently available. The new measurement will take advantage of the improved performances of the Micromegas detector and of the much larger flux available in EAR-2. This last feature is fundamental for studying low cross sections with a reasonable number of protons.

We request 2e18 protons in order to have less than 5% uncertainty in the most significant neutron energy region with a low energy resolution of 10 bin per decade which is enough to fulfil the goals of the present proposal.

We could run in parasitic mode, as we did in 2012 at EAR-1, with other n_TOF experiments at EAR-2

References

- [1] J. Praena *et al.*, for the n_TOF collaboration, *Micromegas detector for $^{33}\text{S}(n,\alpha)$ cross section measurement at n_TOF*. CERN-INTC-2012-006 / INTC-P-322
- [2] G. F. Auchampaugh, J. Halperin, R. L. Macklin *et al.*, *Kilovolt $^{33}\text{S}(n,\alpha)$ and $^{33}\text{S}(n,\gamma)$ cross sections: Importance in the nucleosynthesis of the rare nucleus ^{30}Si* , Phys. Rev. C 12, 1126-33 (1975).
- [3] C. Wagemans, H. Weigmann, R. Barthelemy, *Measurement and resonance analysis of the $^{33}\text{S}(n,\alpha)$ cross section*. Nucl. Phys. A 469, 497–506 (1987)
- [4] G.P. Coddens, M. Salah, J.A. Harvey *et al.*, *Resonance structure of $^{33}\text{S}+n$ from transmission measurements*. Nucl. Phys. A 469, 480–(1987) .
- [5] H. Schatz, S. Jaag, G. Linker *et al.*, *Stellar cross sections for $^{33}\text{S}(n,\alpha)^{30}\text{Si}$, $^{33}\text{S}(n,p)^{36}\text{S}$, and $^{33}\text{S}(n,\alpha)^{33}\text{P}$ and the origin of ^{30}Si* . Phys. Rev. C 51, 379 (1995).
- [6] R. Reifarth, K. Schwarz and F. Käppeler, The Astrophysical Journal, 528, 573-581 (2000).
- [7] I. Porras, *Enhancement of the neutron radiation dose by the addition of ^{33}S atoms*, Phys. Med. Biol. 53, L1-L9 (2008).
- [8] J. Praena, M. Sabaté-Gilarte, I. Porras, J.M. Quesada *et al.*, *^{33}S as cooperative capturer for BNCT*. Appl. Radiat. and Isot. 88, 203 (2014).
- [9] I. Porras, M. Sabaté-Gilarte, J. Praena, J.M. Quesada *et al.*, Nuclear Data Sheets, v 120, 246 (2014).
- [10] NUPECC, Report *Nuclear Physics for Medicine* (2014).
- [11] PW Gout *et al.*, *Increased cystine uptake capability associated with malignant progression of Nb2 lymphoma cells*, Leukemia 11, 1329–1337 (1997).
- [12] Coderre *et al.*, J. Nucl. Med. 27, 1157 (1986).
- [13] ICRU 1978 Dose Specification for Reporting External Beam Therapy with Photons and Electrons ICRU Report 29 (Bethesda, MD: ICRU).
- [14] Y. Giomataris, *et al.*, Nuclear Instruments and Methods in Physics Research A 376 (1996) 29-35.
- [15] M. Asghar and A. Emsallem, Conf: 3.Symp.Neutr.Capt.Gamma Ray Spectr.,Brookhaven (1978) 549.
- [16] J. Benisz, *et al.*, Jour: Acta Physica Polonica, 28 (1976) 763.
- [17] F. Muennich, Jour: Zeitschrift fuer Physik, 153 (1958) 106.
- [18] T. Seppi, Thesis: Seppi (1956). <http://www.nndc.bnl.gov/exfor/servlet/X4sGetSubent?reqx=-1&sub=11422004&plus=1>
- [19] J. Praena *et al.*, for the n_TOF collaboration, *SiMon and Micromegas tests for (n,p) measurements at n_TOF: $^{35}\text{Cl}(n,p)^{35}\text{S}$ and $^{14}\text{N}(n,p)^{14}\text{C}$ Cross Sections*. CERN-INTC-2014-007 / INTC-I-156.
- [20] Wiechers *et al.* [20] Nucl. Phys. A92 (1967) 175-192.
- [21] J. Praena, E. Buendía, F.J. Gálvez and A. Sarsa, Phys. Rev. C 67, 044301 (2003).